Attitude Motion of a Nonattitude-Controlled Cylindrical Satellite

Charles K. Wilkinson*
Textron Defense Systems, Wilmington, Massachusetts 01887

In December 1985, two nonattitude-controlled satellites were each placed in a low-Earth orbit by the Scout launch vehicle. The satellites were cylindrical in shape and contained reservoirs of hydrazine fuel. Three-axis magnetometer measurements, telemetered real time, were used to derive the attitude motion of each satellite. Algorithms are generated to deduce possible orientations (and magnitudes) of each vehicle's angular momentum for each telemetry contact. To resolve ambiguities at each contact, a force model was derived to simulate the significant long-term effects of magnetic, gravity gradient, and aerodynamic torques on the angular momentum of the vehicles. The histories of the orientation and magnitude of the angular momentum are illustrated.

Introduction

THE Scout launch vehicle placed the two satellites into a low-Earth orbit inclined at 37 deg to the equator. Approximately one minute after orbit insertion, the Scout fourth stage/satellite system was despun to about 90 deg/s, and the two satellites were separated sequentially. The separation event imparted lateral rates to the vehicles that modified their angular momentums and coning angles. The coning angles just after the separation event were predicted to be approximately 10 and 50 deg for the respective satellites. Each satellite contained a reservoir of hydrazine fuel amounting to 15% of the total mass. It was expected that energy dissipation from the sloshing fuel would cause the satellites to quickly attain a 90-deg coning angle, i.e., a flat spin about the maximum inertia axis. The satellites are essentially axisymmetric with the minimum inertia axis being the axis of symmetry (see Fig. 1). The maximum inertia axis should be located very close to the Y_G-Z_G plane.

Problem Statement

The problem is to derive each satellite's motion characteristics that are needed to validate and interpret satellite system and mission performance.

Attitude-Related Data

Three-axis magnetometer data are telemetered real time, during contacts, at the rate of 8 samples/s. Figure 2 illustrates the magnetometer data histories (MAGX, MAGY, and MAGZ along the X, Y, and Z axes) for a 7-min contact with vehicle 2 on revolution (Rev) 20.4, approximately 1.3 days after launch. The dropouts and wild points have not been removed from the illustrated data. The equal periodicity on each axis and the small amplitude in the MAGZ data indicate that the satellite is indeed in a flat spin about an axis very near the Z-axis of the satellite. Both vehicles achieved a flat spin prior to the first telemetry contact, which occurred approximately 1 h after launch.

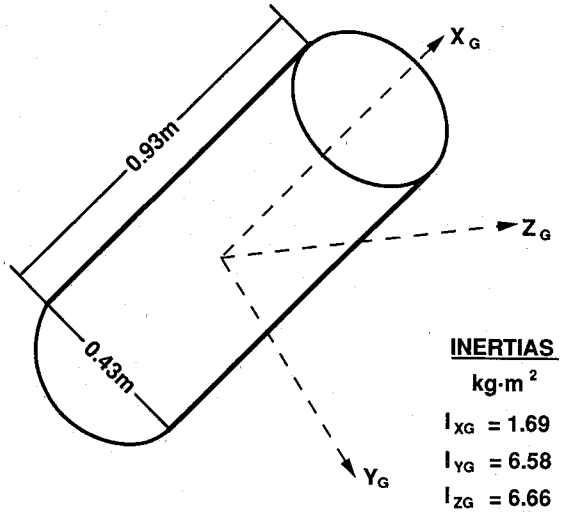

Fig. 1 Satellite configuration.

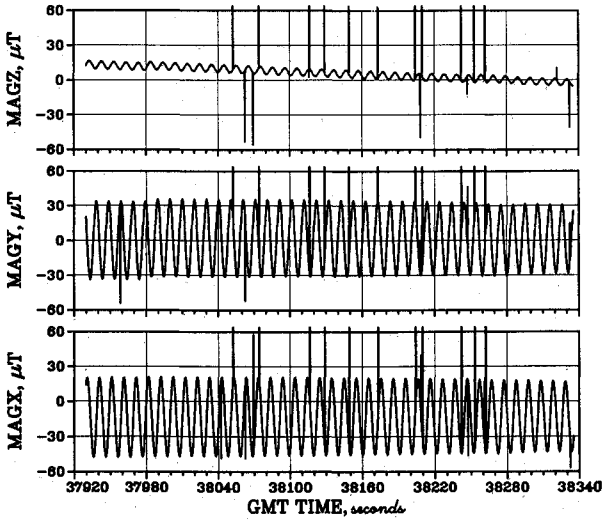

Fig. 2 Magnetometer histories for Rev 20.4, vehicle 2.

Presented as Paper 88-4223 at the 1988 AIAA/AAS Astrodynamics Conference, Minneapolis, MN, Aug. 15-17, 1988; received Oct. 6, 1988; revision received Jan. 13, 1989.

*Principal Engineer, Flight Dynamics Department. Member AIAA.

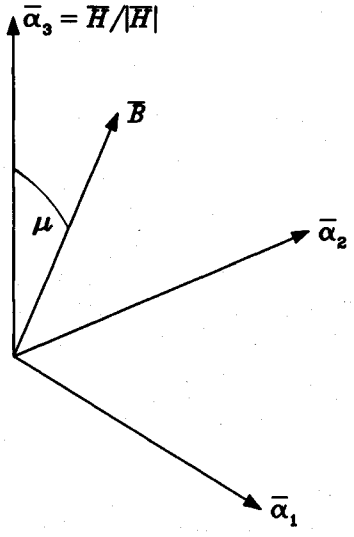

Fig. 3 Instantaneous coordinate system.

The telemetry data are 1) processed in real time for cathode ray tube display and associated hard-copy output and 2) stored on an analog tape for optional postpass processing. Both processing methods convert the raw magnetometer data to engineering units using calibration curves derived on the ground prior to launch. The quantization interval, in engineering units, is 0.472 μT. Real-time hard-copy output of the magnetometer data at a rate of 1 sample/s is routinely available. Since postpass analog tape processing is expensive, a ground-rule was established that the analysis process be compatible with use of the real-time, hard-copy output.

The vehicles were tracked extensively, and accurate orbital elements were readily available and used in the analysis of each contact.

Angular Momentum (Single Contact)

External torques acting on the orbiting satellites are small. Thus, during a short contact, the angular momentum H (referenced to an inertial Newtonian frame) may be assumed to be constant. At a given time t, let $B(t)$ be the magnetic induction vector, and establish a coordinate system $a_1(t)$, $a_2(t)$, and a_3 of mutually perpendicular unit vectors satisfying the following:

a_3 is parallel to H,

$a_2(t)$ is parallel to $a_3 \times B(t)$

$a_1(t) = a_2(t) \times a_3$

The geometry at a given instant in time is illustrated in Fig. 3. Let $\mathcal{P} = (XYZ)$ be the unit vectors of the principal axes coordinate system of the vehicle, with Z the unit vector along the maximum inertia axis and X the unit vector along the minimum inertia axis. For flat-spin motion, Z is parallel to H, i.e., $Z = a_3$. The relationship between the vehicle magnetometer coordinate system $\mathfrak{M} = (X_M Y_M Z_M)$ and $\mathcal{P}$ is illustrated in Fig. 4. The magnetometer axes are designed to be mutually orthogonal and oriented along the vehicle geometric $\mathcal{G}$ frame. The magnetometer data gives no information on the $\mathcal{G}$ frame. We thus work with the $\mathfrak{M}$ frame and assume it is an orthogonal system.

The vehicle motion in principal axes is described by

$$X(t) = a_1(T_0)\cos(\Omega_p t + \psi_0) + a_2(T_0)\sin(\Omega_p t + \psi_0) \quad (1a)$$

$$Y(t) = -a_1(T_0)\sin(\Omega_p t + \psi_0) + a_2(T_0)\cos(\Omega_p t + \psi_0) \quad (1b)$$

$$Z(t) = a_3 \quad (1c)$$

where Ω_p is the precession (flat-spin) rate, ψ_0 the initial precession angle, T_0 the initial time, T the current time, and $t = T - T_0$.

Let ϕ_1, δ, and ϕ_3 be the Euler angle rotations about the X, Y, and Z axes, respectively, defining the transformation, illustrated in Fig. 4, between the $\mathcal{P}$ and $\mathfrak{M}$ frames. The angle δ is assumed to be small since the vehicle is designed to have X_M coincide with X. In the $\mathfrak{M}$ frame, making the small angle approximation for δ and setting $\cos\delta$ to 1:

$$X_M(t) = X(t) + \delta\sin\phi_1 Y(t) - \delta\cos\phi_1 Z(t) \quad (2a)$$

$$Y_M(t) = \delta\sin\phi_3 X(t) + \cos\zeta Y(t) + \sin\zeta Z(t) \quad (2b)$$

$$Z_M(t) = \delta\cos\phi_3 X(t) - \sin\zeta Y(t) + \cos\zeta Z(t) \quad (2c)$$

where $\zeta = \phi_1 + \phi_3$. The vehicle's spin period is short, relative to its translational motion. Thus we assume that B, and therefore a_1 and a_2, are constant over one spin cycle. Then the magnetometer history over one cycle satisfies

$$X_M \cdot B = |B|\left[-\delta\cos\mu\cos\phi_1 - \delta\sin\mu\sin\phi_1\sin(\Omega_p t + \psi_0) + \sin\mu\cos(\Omega_p t + \psi_0)\right] \quad (3a)$$

$$Y_M \cdot B = |B|\left[\cos\mu\sin\zeta - \sin\mu\cos\zeta\sin(\Omega_p t + \psi_0) + \sin\mu\sin\phi_3\cos(\Omega_p t + \psi_0)\right] \quad (3b)$$

$$Z_M \cdot B = |B|\left[\cos\mu\cos\zeta + \sin\mu\sin\zeta\sin(\Omega_p t + \psi_0) + \sin\mu\cos\phi_3\cos(\Omega_p t + \psi_0)\right] \quad (3c)$$

where μ is the angle between H and B. The extrema, $E^{\pm}$, in Eqs. (3) are

$$E_X^{\pm} = |B|(\pm\sin\mu - \delta\cos\mu\cos\phi_1) \quad (4a)$$

$$E_Y^{\pm} = |B|(\pm\sin\mu\cos\zeta + \cos\mu\sin\zeta) \quad (4b)$$

$$E_Z^{\pm} = |B|(\pm\sin\mu\sin\zeta + \cos\mu\cos\zeta) \quad (4c)$$

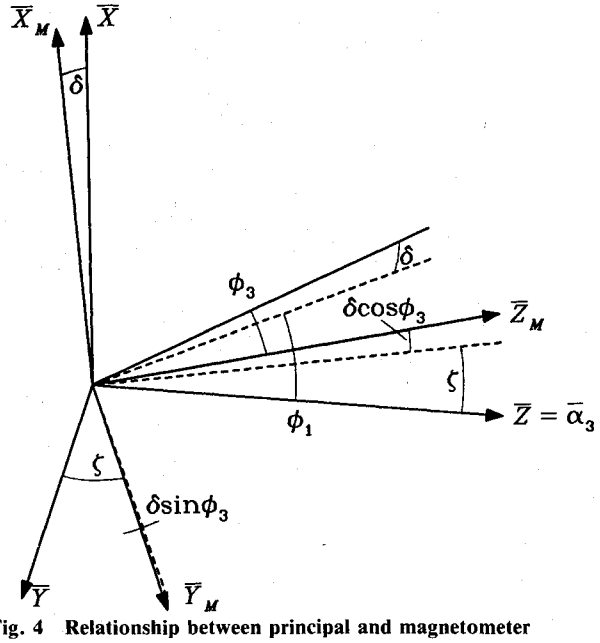

Fig. 4 Relationship between principal and magnetometer coordinates.

Table 1 Computations for Rev 164.2, vehicle 2

	T = 82849 s, GMT[a]			T = 83029 s, GMT			T = 83179 s, GMT		
	X	Y	Z	X	Y	Z	X	Y	Z
$\tilde{E}^+$	−5.2	10.6	38.2	−10.3	7.4	43.0	−6.6	11.3	45.3
$\tilde{E}^-$	−22.8	−7.0	36.3	−17.0	0.7	42.3	−20.6	−2.6	44.0
$\lvert\boldsymbol{B}\rvert$		27.62			30.39			32.92	
ζ		6.2			6.0			5.3	
δ		3.0			2.9			2.6	
μ		18.6			6.3			12.3	
$\tilde{E}^{\pm}$	−1.36	2.82	26.02	−1.52	3.16	30.04	−1.46	2.97	32.03
$\boldsymbol{D}$	−12.64	−1.02	11.23	−12.13	0.89	12.61	−12.15	1.38	12.62
$\hat{\boldsymbol{D}}$	−13.17	0.15	11.30	−12.62	1.61	12.55	−12.62	1.61	12.55

[a]Greenwich mean time.

The extrema $\tilde{E}^{\pm}$ in the observed values, assuming no scaling errors, are

$$\tilde{E}^{\pm} = E^{\pm} + D \tag{5}$$

where $D = D_X X_M + D_Y Y_M + D_Z Z_M$ are the biases along the magnetometer axes. The derivatives of Eqs. (3) are

$$\frac{\mathrm{d}X_M \cdot B}{\mathrm{d}t} = -\Omega_p \lvert B\rvert \sin\mu\left[\delta \sin\phi_1 \cos(\Omega_p t + \psi_0) + \sin(\Omega_p t + \psi_0)\right] \tag{6a}$$

$$\frac{\mathrm{d}Y_M \cdot B}{\mathrm{d}t} = -\Omega_p \lvert B\rvert \sin\mu\left[\cos\zeta \cos(\Omega_p t + \psi_0) + \delta \sin\phi_3 \sin(\Omega_p t + \psi_0)\right] \tag{6b}$$

$$\frac{\mathrm{d}Z_M \cdot B}{\mathrm{d}t} = \Omega_p \lvert B\rvert \sin\mu\left[\sin\zeta \cos(\Omega_p t + \psi_0) - \delta \cos\phi_3 \sin(\Omega_p t + \psi_0)\right] \tag{6c}$$

The occurrences of the extrema are summarized below:

$$X_M \cdot B : \tan(\Omega_p t + \psi_0) = -\delta \sin\phi_1 \tag{7a}$$

$$Y_M \cdot B : \tan(\Omega_p t + \psi_0) = -\cos\zeta/\delta \sin\phi_3 \tag{7b}$$

$$Z_M \cdot B : \tan(\Omega_p t + \psi_0) = \sin\zeta/\delta \cos\phi_3 \tag{7c}$$

Equation (7c) is particularly useful in determining δ when ζ and ϕ_3 are small. In this case ζ is nearly equal to ϕ_1. In any case, the right-hand side of Eq. (7a) is nearly equal to 0.

Procedure for Solving for Attitude Parameters

Determination of an approximate vehicle orientation requires solving for μ, δ, ζ, and D. Since the motion is internally torque free, δ and ζ should be invariant both within a contact and from contact to contact. The D will vary with the vehicle operating configuration, but otherwise should be essentially invariant with time. (It will manifest differences between the actual and modeled magnetic field.) The suggested computation procedure is as follows:

1) Obtain μ from the amplitude in $X_M \cdot B$ [see Eq. (4a)].

2) Obtain ζ from either $Y_M \cdot B$ or $Z_M \cdot B$, whichever has the smaller amplitude [see Eqs. (4b) or (4c)].

3) Equations (7b) and (7c) yield approximations to δ and ϕ_3 from inexact values of t determined from the magnetometer data.

4) Determine $E^{\pm}$ from Eqs. (4).

5) Determine D from Eq. (5).

If $\sin\mu$ is ≈ 1, then an accurate value of μ or D cannot be obtained. The best procedure here is to assume $\sin\mu = 1$, perform steps 2 and 3, and use an average value of D from other contacts to solve for $\cos\mu$ from either of Eqs. (4b) or (4c). With the exception of this case, the magnetometer biases need not be known a priori to solve for μ and ζ.

Determination of Quadrant

The following rules resolve the quadrants of ζ and μ:

$$\mathrm{sgn}(\sin\zeta) = \mathrm{sgn}\left(\frac{\mathrm{d}X_M \cdot B}{\mathrm{d}t}\right) \quad \text{at } t \text{ maximizing } Y_M \cdot B \tag{8a}$$

$$\mathrm{sgn}(\cos\zeta) = \mathrm{sgn}\left(\frac{\mathrm{d}X_M \cdot B}{\mathrm{d}t}\right) \quad \text{at } t \text{ maximizing } Z_M \cdot B \tag{8b}$$

$$\mathrm{sgn}(\cos\mu) = \mathrm{sgn}(\overline{Z_M \cdot B})\ \mathrm{sgn}(\sin\zeta) \tag{8c}$$

Effect of B Variation with Time

In practice, fixing B has little effect on the solutions for μ, ζ, and δ. The variation in $B(t)$ is important in the determination of Ω_p:

$$\Omega_p = \tilde{\Omega}_p + \frac{\mathrm{d}\cos^{-1}[a_1(t) \cdot a_1(t_0)]}{\mathrm{d}t} \tag{9}$$

Specifically, the observed precession rate $\tilde{\Omega}_p$ can be quite different from Ω_p if $H \cdot B$ is small. Further, the values of $a_1(t)$ for the two solutions of H are opposite in sign.

Example 1: $\sin\mu$ is small

Table 1 gives results for the contact on Rev 164 with vehicle 2. The telemetered magnetometer histories are illustrated in Fig. 5. The B values were obtained from an orbit simulation code using a 12-deg spherical harmonic expanison for the geomagnetic potential. The algorithms are used to compute ζ, μ, $(E^+ + E^-)/2$, D, and δ. Independent estimates, $\hat{D}$, for the biases, for comparison purposes, were obtained by an estimation scheme that minimizes, in a least-squares sense, the difference between the magnitudes of the bias-adjusted measured vector and the modeled magnetic induction vector. The values of the biases vary with the operating configuration of the

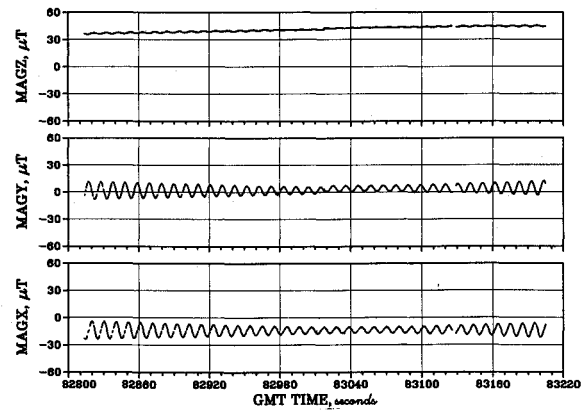

Fig. 5 Magnetometer histories for Rev 164.2, vehicle 2.

Table 2 Computations for Rev 20.4, vehicle 2

	T = 37941 s, GMT[a]			T = 38147 s, GMT			T = 38327 s, GMT		
	X	Y	Z	X	Y	Z	X	Y	Z
$\tilde{E}^+$	20.4	33.7	16.1	20.3	34.6	8.5	17.0	30.7	0.8
$\tilde{E}^-$	−47.4	−33.3	9.8	−45.7	−30.8	2.3	−42.7	−28.4	−4.8
$\lvert B\rvert$		34.09			33.92			33.32	
$\hat{D}$	−13.53	0.17	12.48	−13.08	2.64	13.47	−13.20	2.32	13.05
$\hat{\mu}$		90.0			103.4			116.4	
$\overline{E^{\pm}}$	0.03	0.03	0.47	0.38	−0.74	−8.07	0.45	−1.17	−15.05
ζ		5.3			5.4			5.3	
δ		2.6			2.6			2.6	
μ		89.2			103.8			117.0	
D	−13.47	0.15	12.48	−13.09	2.66	13.47	−13.43	2.55	13.05

[a]Greenwich mean time.

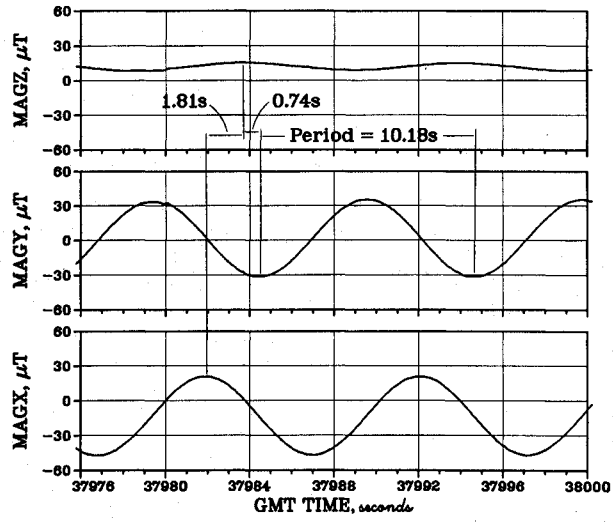

Fig. 6 Magnetometer cycle offset for Rev 20.4, vehicle 2.

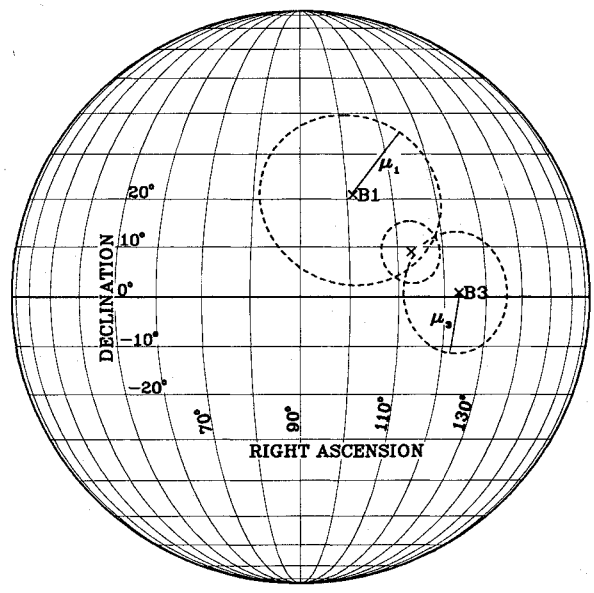

Fig. 7 Potential H orientations: Rev 164.2, vehicle 2.

satellite which is slightly different for each of the three times. The accuracy in δ is poor because of the small variation in $Z_M \cdot B$ and the large quantization interval. The offset in the extrema of $Z_M \cdot B$ from $X_M \cdot B$ and $Y_M \cdot B$ is illustrated in Fig. 6 for Rev 20.4, which gives a larger variation in $Z_M \cdot B$. The satellite rotates about 64 deg between the occurrences of the $X_M \cdot B$ and $Z_M \cdot B$ maxima. This angle was used in Eq. (7c) to solve for δ assuming ϕ_3 is 0. Analysis of several contacts indicated that the values for ζ and δ were close to 5 and 2 deg, respectively. When used in Eqs. (4) and (5), these yield a value of D, which agrees very closely with $\hat{D}$.

Example 2: μ is near 90 deg

It is difficult to determine μ accurately when μ is near 90 deg. Table 2, pertaining to the contact on Rev 20.4 of vehicle 2, illustrates the procedure described above. (Refer to Fig. 2 for the magnetometer histories.) First obtain estimates, $\hat{\mu}$ and $\hat{D}$, of μ and D. Equation (4a) is used to determine $\hat{\mu}$. In general, $\hat{D}$ is an average over several selected contacts. (The value of $\hat{D}$ used in Table 2 was obtained using the aforementioned bias estimation code since the analog tape for that contact was processed postpass.) Then $E^{\pm}$ is determined from Eq. (5), and μ is computed more accurately from Eq. (4c) in the form

$$\cos\mu = \frac{E^+ - E^-}{2\,|B|\cos\zeta}$$

where ζ is obtained by the usual procedure but using $\hat{\mu}$. The other components of D now agree fairly well with those of $\hat{D}$.

Ambiguity in H

The previously described procedure resolves H to lie on a cone of angle μ about B. As the geometry, specifically B, varies with time due to satellite orbital motion, H can be resolved to two points: the intersection of two cones. Over a short contact, the magnetic induction vectors are essentially coplanar. The two possible H vectors are the true H and its mirror image relative to the $B(t)$ plane. The key point is that H cannot be uniquely determined over a short contact. This can be observed very readily in Fig. 7, which illustrates the loci of possible H (minor circles of radius μ_i about point Bi, which is the intersection of B_i with the unit sphere) in right ascension and declination at the three times in Table 1. (A Kalman filter estimation technique designed specifically for this problem could not, in general, decide which of the two possibilities was the correct H orientation.)

The geometry of the two possible H solutions will vary with the orientation of the actual H with respect to the B vectors during the contact. For Rev 21.4, vehicle 1 (Fig. 8), H is quite far from the plane of the $B(t)$ vectors so that the two H possibilities are widely separated. This contact is sufficiently long—7 min—for $B(t)$ to be nonplanar, which allows the correct H to be resolved. On Rev 20.1, vehicle 2 (Fig. 9), H is many degrees from B but is close to the $B(t)$ plane so that, with the uncertainties associated with μ, the possible H values lie along an arc of about 30 deg encompassing declinations from −20 deg to −45 deg. Rev 1.1 for vehicle 1 (see Fig. 10) has similar geometry.

Since the satellite contacts are short, on the order of 3–5 min, and may be separated by about 30 days, other methods must be employed to resolve the ambiguity in the angular momentum orientation. The next section discusses how this issue is resolved.

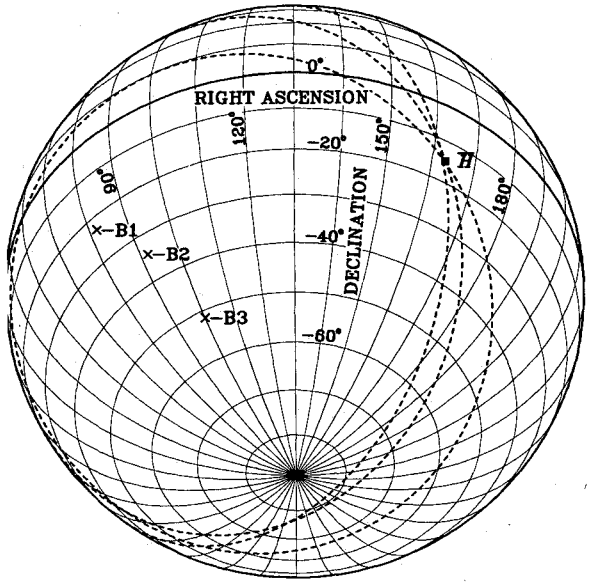

Fig. 8 Resolved H orientation: Rev 21.4, vehicle 1.

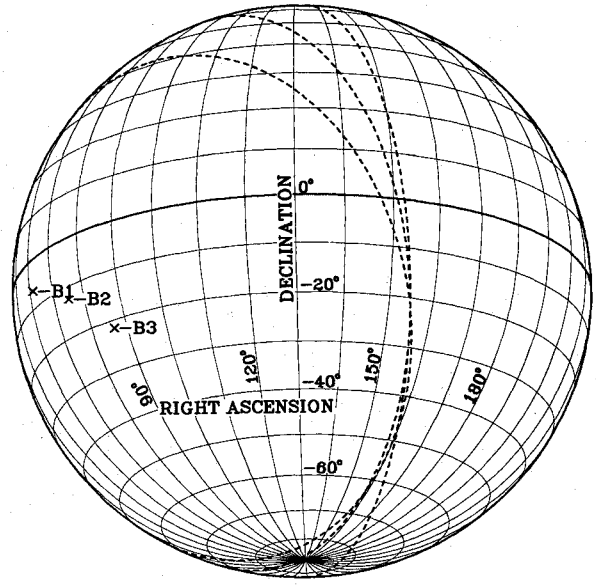

Fig. 9 Potential H orientations: Rev 20.4, vehicle 2.

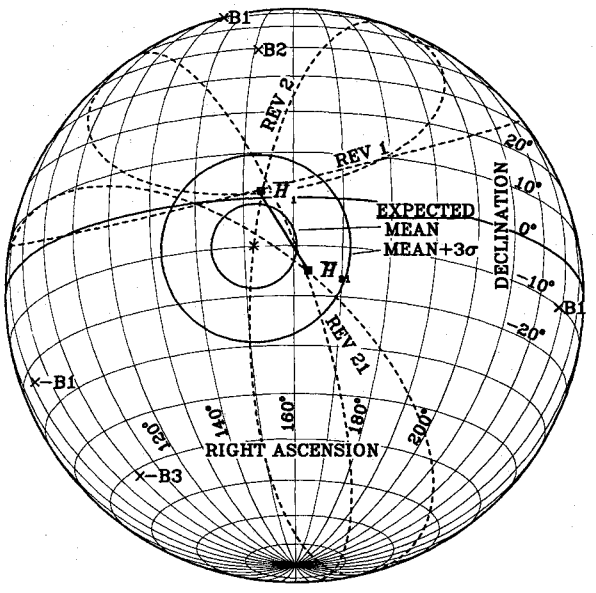

Fig. 10 Resolved H orientations: days 1–2, vehicle 1.

Angular Momentum Resolution

Resolution of the correct angular momentum orientation between the two possibilities requires an initial orientation for H and a torque model from which a long-term history of H can be derived.

Initial Orientation of H

There were frequent contacts with the satellites during the first few days in orbit. Figure 10 illustrates a resolved orientation for the H of vehicle 1 at the intersection of the loci for contacts on Revs 1 and 2. This solution is essentially on the mean of the expected loci determined by a statistical analysis, conducted prelaunch, of the separation of the satellites from the fourth stage of the launch vehicle. Figure 10 illustrates a likely H path from this solution to the H solution on Rev 21. This corresponds to a precession in H of approximately 15 deg/day.

The initial orientation of H for vehicle 2 was established at a right ascension of 162 deg and a declination of -30 deg.

Torque Model

Torques acting on the orbiting satellites originate from magnetic, gravity-gradient, aerodynamic, and solar radiation pressure effects. The approach taken was to obtain expressions, available in the published literature, for the effects on H, of each significant torque over one satellite revolution. These expressions, along with a dipole model of the Earth's magnetic field[5] were incorporated into a semianalytic orbit generation code using a 1-Rev step size. The torque expressions are described briefly next. Because of the small size of the satellites, solar radiation pressure was judged to be a relatively insignificant contributor and was not included in the model.

Magnetic Torques

Magnetic torques result from the interaction between the magnetic properties of a spacecraft and the ambient magnetic field of the Earth. The primary magnetic disturbance torques are the following: 1) dipole moment from the permanent magnetism in the spacecraft; 2) eddy currents induced when a conducting body moves in a magnetic field; 3) spacecraft generated current loops; and 4) hysteresis damping.

Because of the limited amount of spacecraft operating time and the specific amount and properties of permeable material present on the spacecraft, items 3 and 4 were judged to have small contributions to total vehicle torque and were not included in the model.

The torque T_D due to the dipole moment, is normal to $a_3 = H/|H|$ and hence has only a precession component. It satisfies[2,3,5]

$$T_D = m_d a_3 \times B \tag{10}$$

where m_d is the satellite's dipole moment along its Z-axis. Making the assumption that the satellite Z-axis is inertially fixed for an orbital period, the average torque over one orbit Rev satisfies

$$(T_D)_{av} = m_d a_3 \times (B)_{av} \tag{11}$$

The $(B)_{av}$ can be integrated with respect to time over an orbital period[2] to give an average induction vector.

The total torque due to eddy current effects satisfies[5]

$$T_E = k_e(\omega_Z \times B) \times B \tag{12}$$

where k_e is a constant that depends on the geometry and conductivity of the rotating object, and ω_Z is the angular velocity vector of the satellite. Equation (12) can be separated into despin T_{EZ} and precession $T_{E\perp}$, components of torque:

$$T_{EZ} = -k_e(B_\perp)^2\omega_Z \tag{13}$$

$$T_{E\perp} = k_e B_Z B_\perp \omega_Z \quad (14)$$

where $B_\perp$ is the component of B orthogonal to Z, B_Z the component of B parallel to Z, and ω_Z the angular velocity.

These equations are conceptually simple. The complication arises in finding the average values for $(B_\perp)^2$ and $B_Z B_\perp$ over one revolution of the satellite. Reference 3 derived equations for $B_\perp$ and B_Z and then integrated the resulting products. It is easier to resolve $(\omega_Z \times B)\times B$ into its three components, integrate, and then compute the despin and orthogonal components $(T_{EZ})_{av}$ and $(T_{E\perp})_{av}$ of torque. Since the orbit eccentricity is small, terms of $o(e^3)$ and $o(e^4)$ can be deleted.

Gravity Gradient Torque

The average torque over one orbit due to the effect of the Earth's gravitation on the satellite is[1-4]

$$(T_G)_{av} = 1.5\frac{\mu_E}{a^3(1-e^2)^{1.5}}\left(I_Z - \frac{I_X + I_Y}{2}\right)(a_3 \cdot N)(a_3 \times N) \quad (15)$$

where μ_E is the Earth's gravitational constant, a the semimajor axis of the orbit, e the eccentricity of the orbit, and N the unit normal to the orbit plane.

Aerodynamic Torque

The average aerodynamic torque over one satellite spin cycle satisfies

$$T_A = \tfrac{1}{2}\rho v^2 S C_D d(I_v \times a_3) \quad (16)$$

where ρ is the density of the atmosphere, v the velocity of the satellite, S the projected area in the direction of motion averaged over one satellite rotation, C_D the drag coefficient, d the distance from the center of mass of the satellite to its aerodynamic center of pressure along Z averaged over one satellite rotation, and I_v the unit velocity vector of the satellite. The average torque over one orbit was determined using a relatively common procedure[3] for somewhat elliptical orbits.

Spin-Axis Rate Change in One Orbit Revolution

Assuming that the vehicle is in a pure spin motion about the body Z axis, i.e., the principal inertia axis, the change in the spin rate in one orbit revolution caused by the eddy current torque is

$$\Delta\omega_Z = -|(T_{EZ})_{av}|\omega_Z P / I_Z \quad (17)$$

Table 3 Derived magnetic properties

Vehicle	Dipole moment, m_d A − m²	k_e m⁴/Ω
1	+0.543	465
2	−0.230	465

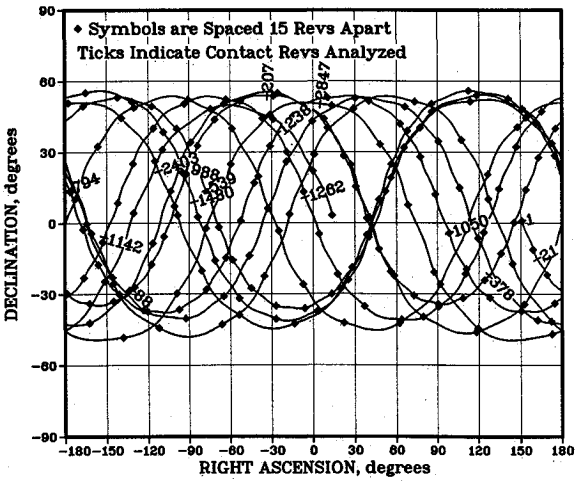

Fig. 11 Evolution of the orientation of H for vehicle 1.

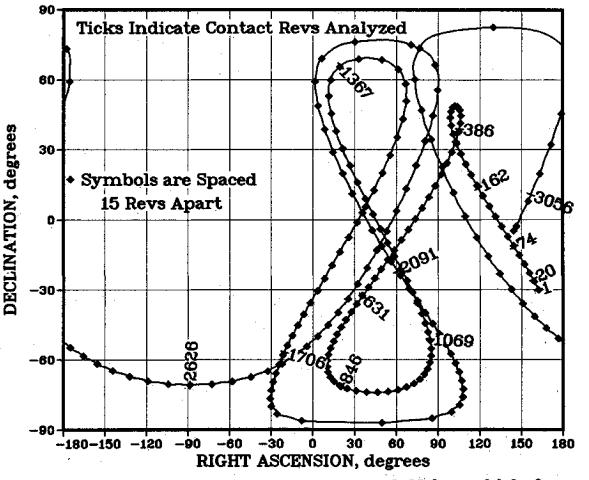

Fig. 12 Evolution of the orientation of H for vehicle 2.

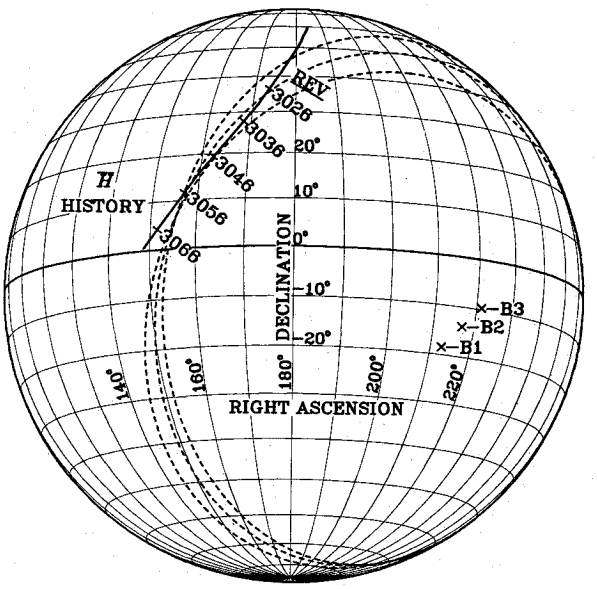

Fig. 13 Simulated vs resolved H: Rev 3056.2, vehicle 2.

where I_Z is the moment of inertia about the body Z axis, and P the satellite orbital period.

Spin-Axis Precession in One Orbit Revolution

Over one orbit Rev, the angular momentum vector H precesses by the angle $|T_{av}|/\omega_Z I_Z$ from H toward T_{av} where T_{av} is the sum of the individual torque contributors normal to H.

Results

With the incorporation of the torque model into the orbit generation code, the determination of approximate values for the key torque-related vehicle-unique properties proceeded rapidly using an iterative simulation process. The inertia properties given in Fig. 1 and an aerodynamic lever arm d of 0.75 cm, equal to the preflight measured center of gravity, offset along the Z_G axis, were used initially for both vehicles. Though they were varied to determine sensitivities, these values were used in the final simulation. The derived magnetic properties are summarized in Table 3.

The dipole moment values are within expectations since satellite magnetic properties were minimally controlled during the design process. The k_e constant should be the same for both vehicles. The derived value is reasonably close to the 600 m⁴/Ω value computed preflight. The gravity gradient and aerodynamic torques had significant effects on the orientation history of vehicle 2 where the dipole moment was much smaller than that for vehicle 1.

The simulated histories of the orientation of H over the first six months in orbit are illustrated in Figs. 11 and 12 for vehicles 1 and 2, respectively. Over this period, the maximum differences between the simulated and calculated H orientations were one day (about 15 Revs) in-track (parallel to the trace of H) and approximately 10-deg cross track (normal to the trace of H). Generally the agreement was much better. Figure 13 illustrates, for Rev 3056 of vehicle 2, typical agreement between the simulation and computations for the orientation of H.

The simulated spin-rate histories are summarized in Figs. 14 and 15. They match the "observed" data very well except for the first few days where the differences are attributed to residual angular momentum in the hydrazine fuel. There appears to be no significant hysteresis in the material magnetization cycle. This would be manifested as a constant component to the primarily exponential spin-decay rate.

Figures 16 and 17 illustrate the histories of the angles between H and N. For vehicle 1, H is never more than 20 deg out of the orbit plane. Its projected area along the flight path, averaged over a spin cycle, is essentially constant. For contrast, the H for vehicle 2 is at times nearly normal to the orbit plane. Thus, its average projected area along the flight path is smaller than that for vehicle 1. This correlates with observed periods of approximately 5% smaller effects of drag on vehicle 2.

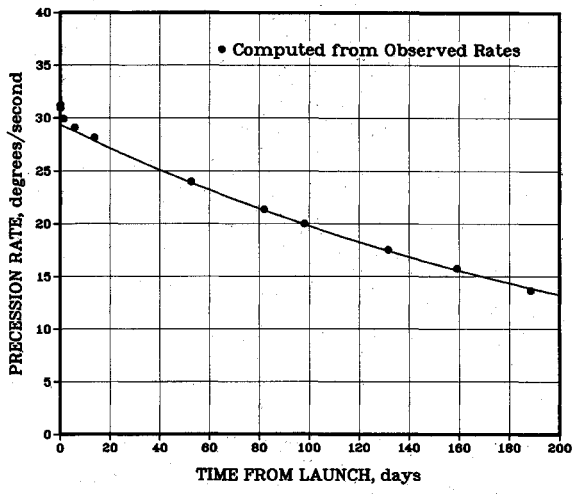

Fig. 14 Precession rate history for vehicle 1.

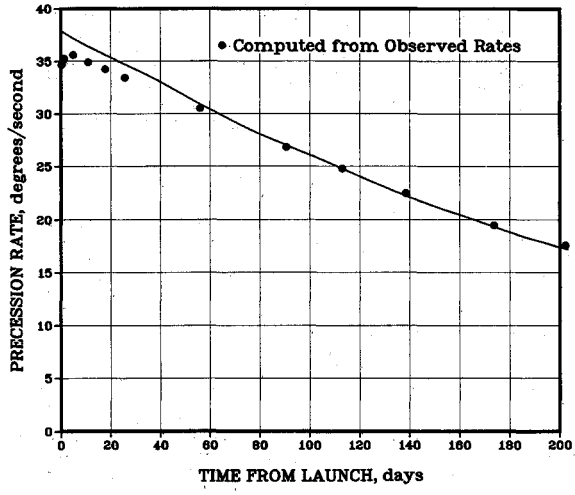

Fig. 15 Precession rate history for vehicle 2.

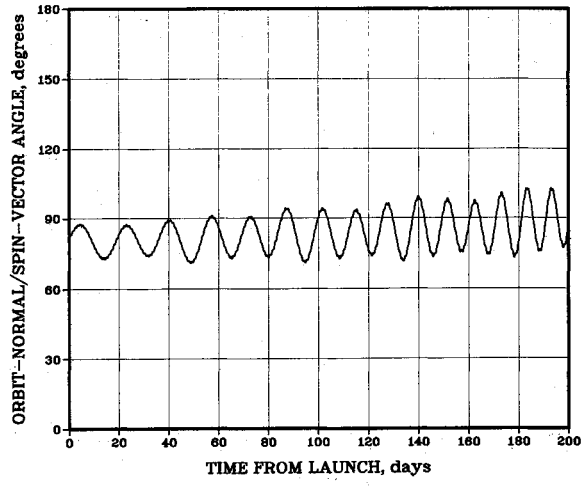

Fig. 16 Angle from H to orbit normal, vehicle 1.

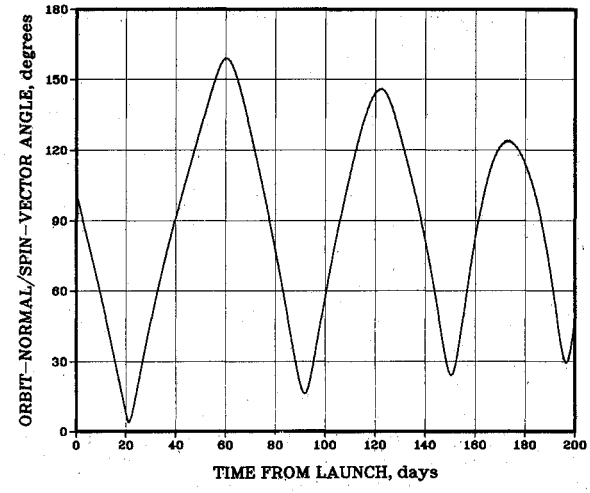

Fig. 17 Angle from H to orbit normal, vehicle 2.

Conclusions

A procedure has been developed to determine the attitude history of two nonattitude-controlled, essentially-axisymmetric spinning satellites using 3-axis magnetometer data only. This data was telemetered real time during contacts of 3–10 min duration, which occurred as infrequently as a month apart. The procedure, which is deterministic, generally resolved the satellite's orientation during a single contact to two possibilities. (Exceptionally, the orientation was resolved unambiguously for some long contacts, but occasionally was uncertain over an arc of 30 to 40 deg length.) The orientation ambiguities were resolved by iterative dynamic propagation of known (gravity gradient) and derived (magnetic and aerodynamic) torques acting on the vehicles. The torques were found to have a significant effect on the time history of the angular momentum vector of the vehicles since the spin rate was low.

The deterministic single-contact procedure was found to be an order of magnitude faster (both in labor and computational requirements) than optimal estimation techniques applied to this problem. These techniques (which were originally looking for a single optimal solution and later modified to find two) also had difficulty in resolving the correct solution on short contacts. They should yield a slightly more accurate solution when the correct orientation is resolved.

No attempt was made to apply optimal estimation techniques to solve for the torques acting on the vehicle. It would be interesting to formulate one that resolved between the two possible orientations on each contact.

Acknowledgment

This work was performed in conjunction with Contract F04701-78-C-0125 for the U.S. Air Force, Space Division. The author is indebted to Richard Heldt of Synetics Corporation (formerly of Textron Defense Systems) for generating, coding, and exercising the bias estimation and Kalman filter codes.

References

[1]Hughes, P. C., *Spacecraft Attitude Dynamics,* Wiley, New York, 1986.

[2]Patapoff, H., "Attitude Drift of a Spin-Stabilized Satellite due to the Earth's Magnetic and Gravitational Fields," *Proceedings of the 14th International Astronautical Congress,* Paris, 1963.

[3]Renard, M. L., "Attitude Perturbations and Magnetic Control for a Spin-Stabilized Satellite," European Space Research Organization, Paris, ESRO TR-1 (ESTEC), Jan. 1966.

[4]Sample, E. C., "A Study of the Spin-Axis Precession Characteristics to be Expected of the S53/UK3 Satellite," RAE TN Space 62, April 1964.

[5]"Spacecraft Magnetic Torques," NASA SP-8018, March 1969.